Journal of Power Sources 196 (2011) 3713–3721

Contents lists available at ScienceDirect

Journal of Power Sources

journal homepage: www.elsevier.com/locate/jpowsour

Catalytic activity of Ni-YSZ anodes in a single-chamber solid oxide fuel cell reactor

Sylvio Savoie [a], Teko W. Napporn [b,1], Bertrand Morel [b,2], Michel Meunier [b], Réal Roberge [a,*]

[a] Institut de recherche d'Hydro-Québec (IREQ), Varennes, Québec, Canada J3X 1S1
[b] Département de Génie Physique, École Polytechnique de Montréal, Québec, Canada H3C 3A7

ARTICLE INFO

Article history:
Received 12 November 2010
Received in revised form
17 December 2010
Accepted 17 December 2010
Available online 8 January 2011

Keywords:
Single-chamber SOFC
Ni-YSZ anode
Catalytic activity
Methane conversion
Selectivity

ABSTRACT

The importance of heterogeneous catalysis in single-chamber solid oxide fuel cells (SC-SOFC) is universally recognized, but little studied. This work presents a thorough investigation of the catalytic activity of three Ni-YSZ half-cells in a well-described single-chamber reactor. One in-house electrolyte-supported and two commercially available anode-supported half-cells composed of anodes with thicknesses ranging from 50 μm to 1.52 mm are investigated. They are exposed to methane and oxygen gas mixtures within CH_4:O_2 flow rate ratios (R_{in}) of 0.8–2.0 and furnace temperatures of 600–800 °C. The conversion of methane always results in the formation of syngas species (H_2 and CO). However, their yields vary considerably based on the individual anode, the operating temperature, and R_{in}. The SC-reactor design and the presence of hot-spots at the reactor entrance bring the methane and oxygen conversion rates well above the limit expected from experiments carried out with anode half-cells only. Major variations in the H_2/CO ratio are observed. In lowering the temperature from 800 °C to 600 °C, it spreads from well below to well above the stoichiometric value of 2.0 expected for the partial oxidation reaction. To optimize the SC-SOFC any further, the findings stress the need to undertake even more catalytic studies of its electrode materials under actual structure and morphology as well as final reactor configuration.

1. Introduction

Catalysis is an essential route to the operation and high performance of single-chamber solid oxide fuel cells (SC-SOFC). Single-chamber cells are usually made of conventional planar SOFC, but unlike dual-chamber configuration, however, both sides of the membrane electrode assembly are exposed to the same ratio of hydrocarbon-to-oxygen flow rates. To explain cell performance, it is then common practice to assume high anode and minimum cathode catalytic conversion of the hydrocarbon fuel [1–6]. This allows the anode to produce large amounts of the electrochemically active syngas species and the cathode to keep most of its active sites free for the electro-reduction of the oxygen gas species at the interface with the electrolyte layer. In reality, however, catalysis at the two single-chamber electrodes is not as straightforward as usually described in the literature. Indeed, early works by Hibino et al. [7] have already shown, for example, that simple anode layers such as nickel and Ni($Ce_{0.8}Gd_{0.2}O_{1.9}$, GDC) exposed to volume ratios of methane:oxygen = 1:1 at 950 °C and open circuit voltage (OCV) give rise not only to H_2 and CO species but also to major quantities of CO_2 gas. Moreover, for cathode components such as $La_{0.8}Sr_{0.2}MnO_3$ (LSM20), they also measured significant oxidation of the methane gas that reaches conversions of about 20%. However, these early catalysis studies were performed under dual-chamber instead of single-chamber conditions.

The catalytic activity of electrode materials has been further studied more recently to account for the SC-SOFC variations in both OCV and maximum power densities. In a conventional flow-through reactor, the catalytic properties of the powder anode material Ni + ($Sm_{0.15}Ce_{0.85}O_{1.925}$, SDC) were studied as a function of temperature for the oxidation of propane under a substoichiometric ratio of C_3H_8:O_2 [8]. The results showed that the ratio of partial oxidation products ($CO + H_2$) to complete oxidation products ($CO_2 + H_2O$) was temperature-dependent with higher quantities of complete oxidation products below 650 °C. Even more studies were performed on the perovskite oxide cathode materials used in SOFC [9–11]. Here, the conversion of methane or propane was investigated as a function of temperature on powder oxides $Ba_{0.5}Sr_{0.5}Co_{0.8}Fe_{0.2}O_3$ (BSCF), $La_{0.2}Sr_{0.8}Co_{0.8}Fe_{0.2}O_3$ (LSCF) and $Sm_{0.5}Sr_{0.5}CoO_3$ (SSC) and found to reach values as high as 20–40%. The materials were leading to the complete oxidation of

* Corresponding author. Tel.: +1 450 652 8172; fax: +1 450 652 8625.
E-mail addresses: savoie.sylvio@ireq.ca (S. Savoie), teko.napporn@univ-poitiers.fr (T.W. Napporn), bertrand.morel@cea.fr (B. Morel), michel.meunier@polymtl.ca (M. Meunier), roberge.real@ireq.ca, roberge_real@yahoo.ca (R. Roberge).
[1] Present address: Laboratoire de catalyse en chimie organique, UMR CNRS 6503, Université de Poitiers, 86022 Poitiers, France.
[2] Present address: CEA-Grenoble, 38054 Grenoble Cedex 09, France.

0378-7753/$ – see front matter © 2011 Elsevier B.V. All rights reserved.
doi:10.1016/j.jpowsour.2010.12.091

the hydrocarbon fuels and to the production of almost 100% CO_2 as the carbon bearing gas species. Finally, other commonly used SOFC materials have been screentested by Riess [12] for their catalytic properties related to the direct chemical reaction.

Unfortunately, the use of oxide powders in conventional flow-through reactors leads to experimental conditions that are very different than in SC-SOFC, especially in terms of flow geometry as well as the structure and morphology of the particulate materials used as the catalyst. Our previous studies on the catalytic activity and performance of symmetrical LSM20 cathode layers in a single-chamber reactor have shown, for example, that the conversion of methane was noticeably dependent on their sintering temperatures [13]. Under flow rates of 450 sccm CH_4:Air mixtures, the LSM20 electrodes sintered at 1200 °C were poorly reactive below an operating temperature of 800 °C. When sintered at 1100 °C, they became reactive at 600 °C, with methane conversion rates reaching values as high as 25% for LSM20 electrodes operated at furnace temperatures of 750 °C.

Modeling of the catalytic reactions inside porous electrodes was also considered by Hao et al. [9,14,15] as part of an elaborate two-dimensional physical model of an SC-SOFC operating on methane fuel. Their work focused essentially on (*i*) the factors responsible for SC-SOFC performance under loading: fuel-to-oxygen ratio, electrolyte material, flow geometry, cell design [9,14]; (*ii*) the numerical investigation of the heterogeneous catalytic reactions inside a 700 μm-thick Ni-YSZ anode running under CH_4:O_2:N_2 = 2:1:4 at 750 °C and maximum power density [15]. In the latter case, Hao and Goodwin's simulation shows three distinct regions of catalytic activity through anode thickness. The results emphasize the major role of water vapour reforming in the production of the electrochemically active hydrogen, and the absence of the partial oxidation reactions of methane in the production of the syngas species.

Although heterogeneous chemistry is acknowledged as a crucial step in the proper functioning of SC-SOFC, the above literature review shows that catalysis has not been quite thoroughly studied under true single-chamber conditions of flow geometry and electrode microstructure. This is surprising given the numerous applications [16], including thermoelectric, for which single-chamber technology is examined, and even more so at a time of intense research activities in SOFC in general for developing new high-performance materials for lower temperature operations. In the case of SC-SOFC, it seems difficult to achieve such a development of materials and ignore the catalytic reactions that are taking place on the preferential sites of the electrode components. This is even more important considering the competition between the catalytic and electrocatalytic conversion processes once the fuel cell is under load.

The present study thus aims to meet some acute research needs in the field of SC-SOFC catalysis. On a fully described single-chamber reactor, the investigation examines the catalytic activity of three Ni-YSZ anode layers of varying thicknesses for their conversion of methane–air gas mixtures. From real-time mass spectrometry (MS) analyses of the exit gas species, the work also assesses the resulting yield and selectivity to H_2, CO and CO_2. The behaviour of the single-chamber reactor is characterized as a function of the anode thicknesses, the incoming ratio of CH_4:O_2 gas flow rates, and the operating furnace temperatures.

2. Experimental

2.1. Materials

The Ni-YSZ catalysts occur in the form of three anode half-cells, all comprising an 8YSZ electrolyte. They consist of an in-house electrolyte-supported half-cell and two commercially available anode-supported half-cells supplied by InDEC B.V. (H.C. Starck) and Forschungszentrum Jülich (FJ), both well-known developers of SOFC components.

The in-house anodes consist of two layers: (*i*) a thicker 45 wt% NiO/55 wt% 8YSZ as a functional layer and (*ii*) a thin NiO coating added as a contact layer. The respective NiO (Baker) and 8YSZ (Tosoh) powders are first mixed and turned into an ink through the addition of triton (dispersant), terpineol (solvent), and PVB (binder) [13,17]. The layers (approximately 14 mm × 23 mm) are applied through a Doctor Blade technique on a 500-μm-thick 8YSZ membrane measuring 16 mm × 25 mm. The functional layer is applied first and dried at 150 °C before the addition of the NiO coating. Final sintering of the layers is performed for 3 h at 1375 °C. The total thickness of the in-house anode is around 50 μm.

The state-of-the-art anode-supported half-cells consist of NiO/8YSZ bilayers where a thin functional layer (≤10 μm) is applied between the assumed gastight electrolyte (<20 μm) and the much thicker NiO/8YSZ anode substrate. The latter notably serves as the mechanical-supporting component of the cell. Each layer has its own composition and morphology for appropriate electrochemical conversion and fuel gas flow when operated under solid oxide fuel cell conditions in a complete cell. For our purpose, the most important difference between the two half-cells resides in the thickness of their anode layers. The InDEC half-cells have a total anode thickness of about 0.56 mm. The FJ ones are much thicker at about 1.52 mm. This increase in thickness allows FJ to manufacture a more porous anode substrate. No further in-depth examination was, however, performed to characterize these individual cells in terms of composition and microstructure. The as-received components measured 16 mm × 25 mm.

In the following sections, the respective in-house electrolyte-supported half-cell and the two anode-supported half-cells will be referred to as the InHo-0.05-mm-, InDEC-0.56-mm- and FJ-1.52-mm anodes according to their origins and thicknesses.

2.2. Single-chamber reactor

Fig. 1(a) presents a section of the single-chamber reactor setup. The fuel half-cell and the gas distribution plates (GDP) are first located inside a holder attached at the extremity of an internal tube. To simulate an operating single-chamber reactor, gold mesh current collectors (not shown) are also placed on both sides of the half-cell and between the GDP. A screw in the holder firmly presses against the half-cell, current collectors and GDP. The holder, plates and internal tube are all made of alumina. This assembly is slid into a quartz tube, and the whole assembly is then placed into a tube furnace (not shown). A thermocouple pressed onto the half-cell on its entry side, but outside the internal tube, serves to measure the mean temperature. It is ceramic-coated to avoid any possible catalytic effects. The internal tube is used as the fuel inlet port to the cells. The external tube carries Ar gas at a flow rate of 700 sccm to dilute and transport the exiting fuel and reaction products from the half-cell holder. The external tube is connected to a quadrupole mass spectrometer (QMS, model Prisma©from Pfeiffer-Balzers) for gas analysis. In between and outside the furnace, a gas mixer (not shown) ensures proper mixing of the outlet gas species.

As shown in Fig. 1(b), the bottom gas distribution plate rests on a shoulder made into the cell holder, whereas the top plate is left loose for the half-cell assembly in-between. In all cases, and as schematically shown in Fig. 2 for the InDEC-0.56-mm anode, the anode layer is facing down onto the bottom plate. Finally, the GDP (16 mm × 25 mm) contain regularly spaced posts (Fig. 1(c)) that uniformly mix the gas over the half-cell components. Important leakage of the gas species is prevented by the use of solid walls around the edges. However, small leakage into the free space in the cell holder is still possible since, as explained above, the half-cell and the current collectors are simply pressed between

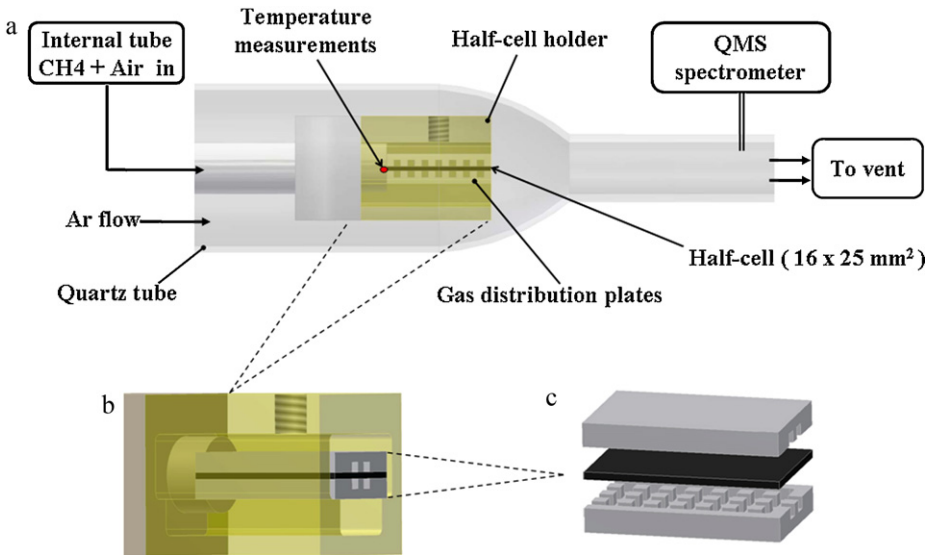

Fig. 1. (a) Section view of the single-chamber SOFC setup; (b) 3-D view of the half-cell holder; (c) exploded view of the half-cell and gas distribution plates.

the GDP. The outlet face has two ports for the exhaust gas species and the connecting gold wires. These GDP plates were successfully tested before on electrolyte-supported Ni-YSZ/YSZ/LSM cells fed with methane gas [18]. The plates, the current collectors and the cell form the so-called SC-SOFC reactor once a complete cell is in use. The free volume above each side of the components is about 0.34 cm^3.

2.3. Catalytic testing

The single-chamber reactor is operated at furnace temperatures of 600 °C, 700 °C, and 800 °C. The inlet fuel is made of methane/air mixtures kept at a constant total flow rate of 450 sccm. The catalytic activity measurements are carried out as a function of CH_4:O_2 flow rate ratios (R_{in}), ranging from 0.8 to 2.0. More specifically, the following R_{in} (CH_{4in}:O_{2in}, sccm) conditions are studied: 2.0 (128.6:64.3); 1.6 (109.1:68.2); 1.2 (87.1:72.6); 1.0 (75.0:75.0); 0.8 (62.1:77.6).

The QMS spectrometer is operated in a multi-channel mode for real-time analyses of CH_4, H_2, CO, CO_2, O_2, and H_2O. However, condensation along the walls prevents the water species from being directly quantified. In the air mixture, nitrogen is replaced with a mixture of Ar–5% He to avoid any overlapping of its mass unit

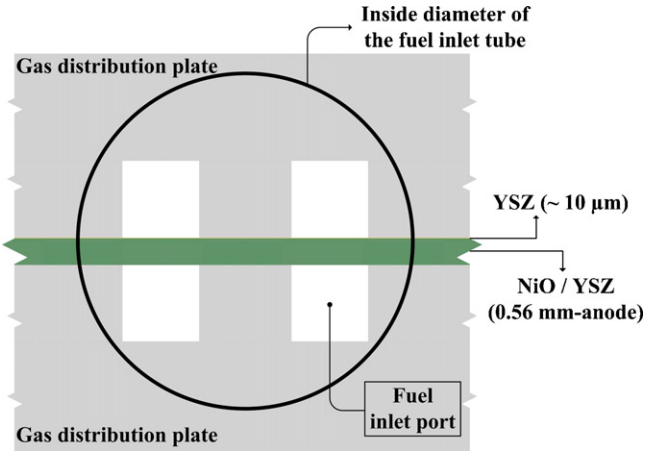

Fig. 2. Front view of the SC-SOFC reactor entry side showing the InDEC-0.56-mm anode half-cell.

$m/z = 28$ feature with the cracking patterns of CO and CO_2. The intensity of the measured signals are normalized to that of He gas and calibrated in flow rates, taking into account the background of the individual signals in flowing Ar–5%He gas mixtures alone. Blank tests including a mounted YSZ electrolyte have been performed to confirm the negligible effect of the single-chamber components in the combustion of the fuel mixtures.

The results are expressed in terms of CH_4 and O_2 conversation rates and yields of H_2, CO and CO_2, all in percentages, according to the following relations:

$$X_{CH_4} = \frac{(CH_{4in} - CH_{4out}) \times 100}{CH_{4in}} \quad (1)$$

$$X_{O_2} = \frac{(O_{2in} - O_{2out}) \times 100}{O_{2in}} \quad (2)$$

$$Y_{H_2} = \frac{H_{2out} \times 100}{(2 \times CH_{4in})} \quad (3)$$

$$Y_{CO} = \frac{CO_{out} \times 100}{CH_{4in}} \quad (4)$$

$$Y_{CO_2} = \frac{CO_{2out} \times 100}{CH_{4in}} \quad (5)$$

They also are discussed against the selectivity (%), S_i, to hydrogen and carbon monoxide, as well as the H_2/CO ratio defined as

$$S_i = \left(\frac{Y_i}{X_{CH_4}}\right) \times 100 \quad (6)$$

$$\frac{H_2}{CO} = \frac{2 \times Y_{H_2}}{Y_{CO}} \quad (7)$$

Before the start of the experiments, the half-cell is first heated at a nominal temperature of 700 °C and the anode reduced in argon/methane mixtures. Short reduction times are applied according to the procedure developed earlier [19]. With CH_4 flow rates of 109.1, the time to reduction was around 6.5 min for the InHo-0.05-mm anode, 25.0 min for the InDEC-0.56-mm anode, and 18.5 min for the FJ-1.52-mm anode. At the end of the reduction process, air is introduced and the CH_4:O_2 flow rate ratio adjusted to 2.0. The catalytic activity measurements at 700 °C are then carried out in sequence at every R_{in} ratio from 2.0 to 0.8. Data analysis is performed once stability in the QMS signals is obtained. The catalytic activity is subsequently examined in order at 600 °C and 800 °C.

Table 1
Mass spectrometry results for the three Ni-YSZ anode catalysts at furnace temperatures of 600 °C, 700 °C and 800 °C as a function of R_{in} (450 sccm total flow rate).

Ni-YSZ anode	R_{in}[a]	600 °C					700 °C					800 °C				
		Conversion, %		Yield, %			Conversion, %		Yield, %			Conversion, %		Yield, %		
		CH_4	O_2	H_2	CO	CO_2	CH_4	O_2	H_2	CO	CO_2	CH_4	O_2	H_2	CO	CO_2
InHo-0.05-mm	2.0	22	46	12	12	10	33	58	18	25	7	43	73	21	34	6
	1.6	28	46	16	16	13	39	58	19	27	10	46	71	18	32	10
	1.2	33	43	16	15	18	38	51	16	21	17	47	63	14	27	17
	1.0	28	36	11	9	20	36	45	12	15	21	43	52	10	20	20
	0.8	20	24	6	4	18	27	31	6	6	22	31	33	6	10	20
InDEC-0.56-mm	2.0	27	54	16	13	13	38	62	25	28	9	52	85	31	42	9
	1.6	33	52	20	17	16	46	63	28	31	13	56	83	27	38	15
	1.2	39	50	21	16	22	47	59	23	25	21	61	79	23	35	23
	1.0	37	47	16	11	27	46	54	18	19	26	62	73	18	30	28
	0.8	31	37	8	5	29	36	42	9	8	30	44	48	9	14	29
FJ-1.52-mm	2.0	48	87	31	28	18	64	94	46	51	11	73	94	57	64	7
	1.6	59	86	39	36	23	73	94	50	55	17	74	95	51	58	15
	1.2	69	84	43	36	34	75	94	39	44	31	76	95	38	47	28
	1.0	71	82	36	27	42	76	91	34	35	41	79	94	31	39	39
	0.8	68	75	25	17	51	75	83	23	23	51	82	90	20	29	52

[a] Ratio of CH_{4in} to O_{2in} flow rates (see Section 2.3).

Typically, before any new sequence of tests, the anode is reoxidized in oxygen and reduced again either at 700 °C, before the tests at 600 °C, or at 800 °C. The same reduction procedure described above is followed but the time to reduction may differ. When appropriate, the half-cell is left in a flowing mixture of Ar/He to prevent any reoxidation before the new sequence of measurements. After the tests at 600 °C and 800 °C, the catalytic activity of the anode is again examined at 700 °C to confirm its initial performance.

3. Results and discussion

Table 1 provides a comprehensive overview of the catalytic performance found with the three Ni-YSZ anodes at the furnace temperatures of 600 °C, 700 °C and 800 °C. The results for the individual anode layers appear in the form of conversion rates of the fuel mixture (CH_4 and O_2), and yields of the formed products (H_2, CO and CO_2) at every CH_4:O_2 flow rate ratio studied. They are more thoroughly presented in the next two sections which deal first with an analysis of the reaction products measured at the reactor outlet, and second with the catalytic activity of the Ni-YSZ anodes. A third section examines the selectivity to the partial oxidation products and the H_2/CO ratios for assessing the possible processes involved in the single-chamber reactor.

3.1. Yield of combustion products

An examination of Table 1 reveals that the catalytic conversion of methane in the SC-reactor gives rise to the formation of H_2, CO and CO_2 gas species, the ratios of which vary according to the CH_4:O_2 fuel mixture and the furnace temperature. Starting with the partial oxidation products, the yields in H_2 and CO tend to increase with an increase in R_{in}. This is especially true at 800 °C (Table 1) which also results for every half-cell in the largest production of syngas at R_{in} = 2.0. There, Y_{H_2} ranges from about 21% to 57% in passing from the InHo-0.05-mm anode to the FJ-1.52-mm anode. Similarly, Y_{CO} goes from about 34% to 64%. At lower temperatures, the yields show a short maximum between the ratios 1.2–1.6 at 600 °C, and 1.6–2.0 at 700 °C. Comparing the individual anode layers at fixed values of R_{in} shows that a rise in furnace temperature always results in an increasing amount of CO gas species. For hydrogen, however, this is true only at CH_4:O_2 = 2.0. At lower ratios, the yield in H_2 rather shows a levelling out or even a decrease of its value.

The conversion of CH_4 also results in total oxidation products. Although the production of CO_2 is not significantly affected by the operating temperature of the SC reactor, it is however strongly dependent on the R_{in} ratio. In fact, its yield steadily increases with a rise in the oxygen content of the reactant gas mixture. In general, it tends to level out at the lowest ratios except for the FJ-1.52-mm anode, where a steady increase is observed down to R_{in} = 0.8. In every case, however, the yield in CO_2 total combustion product clearly prevails at the lowest CH_4:O_2 ratios and even more so when the operating temperature is at its lowest value.

Fig. 3 shows a comparison of the typical behaviour observed in the yields of the measured combustion products, taking as an

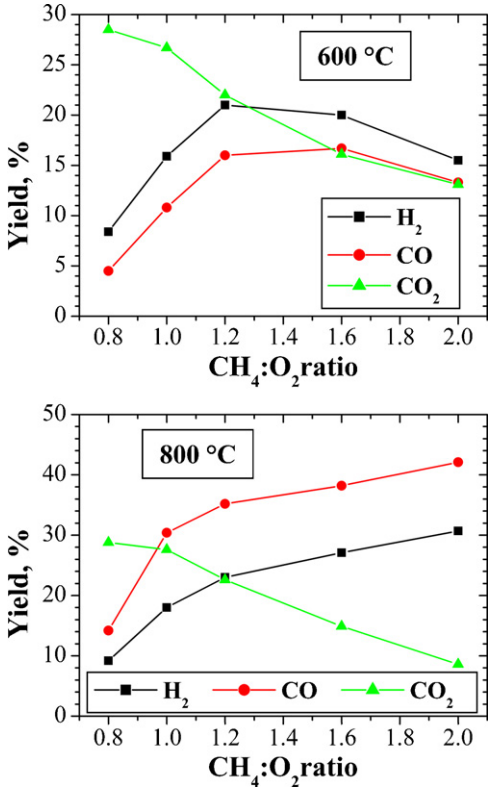

Fig. 3. Typical variation in the yields of H_2, CO and CO_2 as a function of the CH_4:O_2 fuel flow rate ratio measured at a furnace temperature of 600 °C and 800 °C for the InDEC-0.56-mm anode.

example the InDEC-0.56-mm anode at a furnace temperature of 600 °C and 800 °C.

As shown with the previous results, it is not strictly accurate in SC-SOFC to always assume a large production of the electrochemically active H_2 and CO gas species at the anode surface. Notably with Ni catalysts, the partial oxidation reaction of methane is a complex process. In the past, two catalytic pathways have been usually proposed [20,21]: (i) the direct partial oxidation mechanism (8), and (ii) the combustion and reforming reactions mechanism (9)–(11).

$$CH_4 + 1/2O_2 \rightarrow CO + 2H_2 \quad (8)$$

$$CH_4 + 2O_2 \rightarrow CO_2 + 2H_2O \quad (9)$$

$$CH_4 + H_2O \rightarrow CO + 3H_2 \quad (10)$$

$$CH_4 + CO_2 \rightarrow 2CO + 2H_2 \quad (11)$$

Moreover, the propensity in forming the partial or the total oxidation products depends largely on the chemical state of the Ni catalyst. In the presence of metallic nickel (Ni) only, for example, a high yield of synthesis gas and selectivity to CO gas species often larger than 95% is obtained [22–25]. However, in any catalytic reactor, both the reduced and the oxidized forms may coexist depending on experimental conditions such as temperature, flow rate, CH_4:O_2 ratio, gas distribution, heat and mass transport. With increasing amounts of oxidized catalyst particles, the likelihood of forming both the partial and the complete oxidation products increases since the methane fuel may now also interact with the lattice oxygen of the NiO species through the following oxido-reduction process [22–27]:

$$CH_4 + 4NiO \rightarrow CO_2 + 2H_2O + 4Ni \quad (12)$$

$$2Ni + O_2 \rightarrow 2NiO \quad (13)$$

In single-chamber experiments, the CH_4:O_2 fuel mixture that feeds the cell is an obvious factor in the existence of both the Ni and the NiO phases. In the present investigation, however, these two phases may also be promoted right from the beginning by the reduction processes applied before every catalytic activity sequence of measurements. Indeed the very short time allowed in reducing the nickel oxide in argon/methane mixtures (see Section 2.3) probably does not allow a full reduction of the sintered NiO-YSZ anode layers. Under those conditions, the combustion of CH_4 may thus proceed on both the Ni and NiO phases, the ratio of which is largely regulated by the oxygen content of the fuel mixture and its conversion during the catalytic processes. Lowering the CH_4:O_2 ratio could favour the formation of NiO and result in a more significant production of CO_2 below R_{in} = 1.4–1.6. Although it is not easy to properly reduce the anode of a SC-SOFC by in situ processes [28], a successful procedure that would leave larger amounts of Ni could possibly lead to higher yields in partial oxidation products and better electrochemical performance of complete SC-SOFC cells. While it is reasonable to believe in non-uniform composition of the catalyst layer along the single-chamber reactor, further studies to characterize the active nickel phase under the actual reaction conditions and various oxygen conversion levels should be undertaken. Similarly, long-term experiments may be required to examine the possibility of reducing completely the remaining NiO, especially under conditions where total oxygen conversion at the fuel cell entrance occurs.

The usual criteria in SC-SOFC is to normally operate the fuel cells at R_{in} values between 1.6 and 2.0 where the H_2 and CO gas species are expected to be at their highest level of production. Although this may be true at high temperature, our results on Ni-YSZ catalysts show that yields in CO_2 as important as those found for the partial oxidation products may be observed with a reduction in furnace temperature. The case at 600 °C for the InHo-0.05-mm and InDEC-0.56-mm anodes is notably typical (Table 1). While in dual-chamber

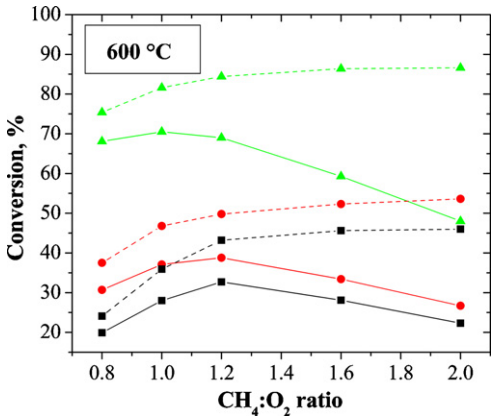

Fig. 4. Conversion of methane and oxygen as a function of the CH_4:O_2 fuel flow rate ratio at an operating temperature of 600 °C. Solid lines: X_{CH_4}; dashed lines: X_{O_2}. Black squares: InHo-0.05-mm anode; red circles: InDEC-0.56-mm anode; green triangles: FJ-1.52-mm anode. (For interpretation of the references to color in this figure legend, the reader is referred to the web version of the article.)

SOFC the tendency is to actually reduce the working temperature of the fuel cells, in the case of the single-chamber SOFC one has to be aware that too large a reduction may significantly decrease the production of H_2 and CO gas species in favour of the more complete oxidation products. Such dilution of the electrochemically active species may result in a lower performance of the fuel cells.

3.2. Conversion

The general trends observed in the conversion rates of methane and oxygen as a function of the CH_4:O_2 ratio is given in Fig. 4 at an operating temperature of 600 °C. From R_{in} = 2.0, a decrease in the methane content of the fuel mixture initially produces an increase of its conversion generally down to a ratio of 1.2–1.0. This is typical for the CH_4 combustion on metal catalysts such as Ni, Rh and Pt [29–32], and in agreement with a reaction process that is limited by the supply of oxygen to the catalytic sites. Below these threshold values, we generally witness an obvious decline of the CH_4 conversion rates, except for the FJ-1.52-mm anode. In the latter case, the slight decrease observed at 600 °C (Fig. 4) progressively transforms, at 800 °C, into a continual increase in X_{CH_4} down to R_{in} = 0.8 (Table 1). The strong interaction between nickel and oxygen, and the extent to which the latter is converted during the catalytic processes, explain the behaviours observed above. In the presence of incomplete O_2 conversion reactions, as in the InHo-0.05-mm and InDEC-0.56-mm anodes, any excess in oxygen may be used to re-oxidize the metallic nickel into NiO and induce a fall in X_{CH_4}. When X_{O_2} approaches 100% as for the FJ-1.52-mm anode at 800 °C, there is no more excess in oxygen, and the nickel catalyst is left in its most favourable metallic state for the conversion of methane.

As also shown in Fig. 4, the oxygen conversion is much larger than the methane's at the highest CH_4:O_2 ratios. The difference is reduced when going to lower ratios, and almost disappears at R_{in} = 0.8. However, as the experiments are performed at a constant total flow rate of the fuel-air mixture, the mole fraction of oxygen-to-methane converted (O_{2Conv}/CH_{4Conv}) in fact increases significantly with a decrease in the CH_4:O_2 ratio. This is shown in Fig. 5 for the three Ni-YSZ anodes at an operating temperature of 800 °C. In this case, the mole fraction steadily rises from about 0.60–0.85 at R_{in} = 2.0, to a maximum of about 1.35 at R_{in} = 0.8. At lower temperatures, the trends are similar except for a levelling of the mole fraction at $R_{in} \geq 1.6$. At 600 °C, this plateau-value of the mole fraction ranges from about 0.9 to 1.0 in going from the FJ-1.52-mm anode to the InHo-0.05-mm one. Overall, the O_{2Conv}/CH_{4Conv} mole fraction nears the stoichiometric value of the partial oxidation

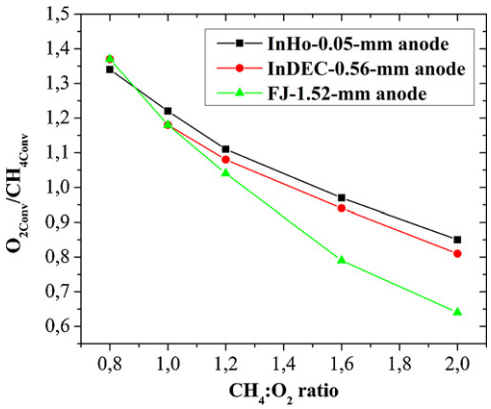

Fig. 5. Variation of the mole fraction of oxygen-to-methane converted as a function of the CH_4:O_2 fuel flow rate ratio at an operating temperature of 800 °C.

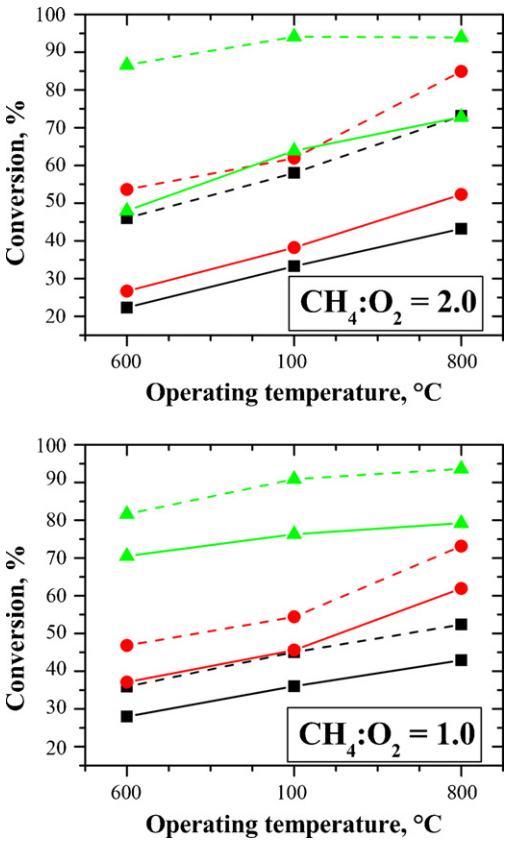

Fig. 6. Conversion of methane and oxygen at CH_4:O_2 = 2.0 and 1.0 as a function of the operating temperature between 600 °C and 800 °C. Solid lines: X_{CH_4}; dashed lines: X_{O_2}. Black squares: InHo-0.05-mm anode; red circles: InDEC-0.56-mm anode; green triangles: FJ-1.52-mm anode. (For interpretation of the references to color in this figure legend, the reader is referred to the web version of the article.)

reaction of methane at high temperature and R_{in} ratio. A decrease in both parameters, but especially in R_{in}, gives rise to more complete oxidation reactions and to an increase in the O_{2Conv}/CH_{4Conv} mole fraction, confirming the results of the previous section on the yields of the reaction products.

Besides the typical variations with the CH_4:O_2 ratio, however, Fig. 4 also shows very high conversion rates as well as major differences among the three anode layers. At 600 °C and R_{in} = 1.2, for example, the InHo-0.05-mm and InDEC-0.56-mm anodes oxidize respectively about 33% and 39% of the CH_4 fuel. On the FJ-1.52-mm anode, however, X_{CH_4} reaches 70%. Clearly, with values between about 75% and 85% in the whole range of CH_4:O_2 ratio studied X_{O_2} also shows the same sudden increase when going to the larger anode layer. Since the incoming fuel is in principle split between an active anode layer and an inert YSZ electrolyte (see the Sections 2.2 and 2.3), such high values are well above the 50% limit expected for 100% conversion in experiments performed with only one reacting chamber. Moreover, on the less reacting anode catalysts, X_{O_2} is already reaching values near or even slightly above this 50% limit at the highest R_{in} ratios. Surprisingly, these results are obtained at the lowest operating temperature of 600 °C, while any increase in temperature is expected to raise the catalytic activity even further. This temperature effect is shown in Fig. 6 for the two limiting cases of the CH_4:O_2 ratio inside the range $1.0 \leq R_{in} \leq 2.0$ for syngas production. The sharp increase observed earlier in the conversion of methane and oxygen in going to the FJ-1.52-mm anode generally remains with an increase in the operating temperature. The only exception is in comparison with the InDEC-0.56-mm anode. Indeed, the latter shows, especially at R_{in} = 1.0, a more significant raise in the conversion of methane and oxygen gas species as the temperature is increased from 700 °C to 800 °C. Furthermore, at 800 °C and R_{in} = 2.0, the total conversion of oxygen on the InHo-0.05-mm and InDEC-0.56-mm anode layers rises to 73% and 85%, respectively. The high rates observed in X_{O_2} could initially suggest the production of totally inadequate conditions for the successful operation of a complete fuel cell, especially if the cathode itself is somehow catalyzing the fuel mixture. However, earlier studies of an InDEC-0.56-mm anode-supported Ni-YSZ/YSZ/LSM fuel cell performed in a very similar SC-reactor have shown quite typical cell behaviour and high electrical performance [33]. Supposedly here, the presence of a cathode may change the conversion features among the two chambers possibly by altering the heat transfer processes.

Various factors may contribute to the extreme conversion noticed above and cause the step-rise increase in performance observed on the FJ-1.52-mm anode catalyst. Among these, the changes in frontal surfaces and the specific design of the actual single-chamber reactor are possibly the most critical ones. As shown in Fig. 2, the incoming fuel mixture, in entering the reactor, is facing the fuel half-cell as well as the two gas distribution plates. In this configuration, the latter are forming large impermeable solid surfaces that actually work as baffle-plates. They give rise to an enhance mixing in front of the cell and to an increased mass transfer of the CH_4:O_2 gas species to the most active sites of the anode surface. At steady-state, these active sites are found at the reactor entrance and especially at the frontal surface. This results in significant temperature gradients (hot spots) under the effect of the exothermic partial and complete oxidation reactions. Such phenomena are well known in the catalytic oxidation of methane [34–38], and often lead to catalyst deactivation. The improved mass transfer process is probably sufficient by itself to raise the methane and oxygen conversion rates to their expected maximum values. However, when we further add the noticeable increase in frontal surface area of the anode layers, from the thin InHo-0.05-mm to the thick FJ-1.52-mm anode, these rates can now come close to or even exceed the 50% limit expected for the actual reactor configuration. Of course, other internal parameters such as the structure and morphology of the individual catalyst layers, for example, will modulate the conversion rates and lead to the recorded values.

The previous assertion still does not explain the gap observed between the InDEC-0.56-mm and the FJ-1.52-mm anode, for example. Under SC-SOFC conditions, however, the presence of hot spots also results in significant mechanical stresses in the Ni-YSZ/YSZ half-cell due to the large mismatch between the thermal expansion coefficients of the anode and electrolyte components. Serious outcomes can result such as leakage of the feeding gases through the cell materials and, in the worst case scenario, mechanical failure. This will noticeably take place on cells made of thin and brittle

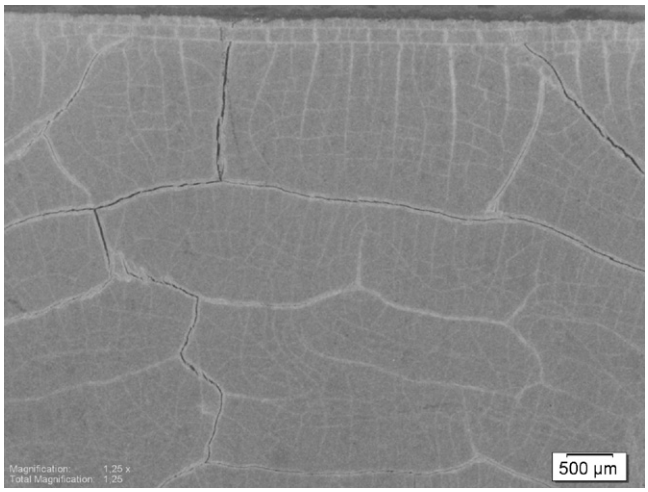

Fig. 7. Optical microscopy image of the cracking pattern observed on the FJ-1.52-mm anode-supported half-cell.

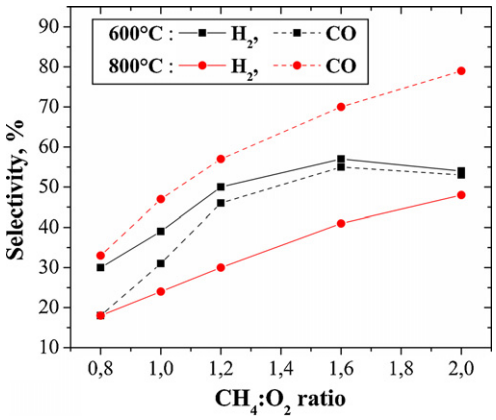

Fig. 8. Selectivity to H_2 and CO as a function of the CH_4:O_2 flow rate ratio at 600 °C and 800 °C: InHo-0.05-mm anode.

electrolyte layers such as those found on the InDEC-0.56-mm and FJ-1.52-mm anode-supported half-cells. Post-mortem examination of the latter under optical microscopy in fact suggests a cracking pattern (Fig. 7) on the YSZ electrolyte that could originate at the inlet and progress as far as 7–9 mm downward. According to the results, crack initiation should occur as early as in the first sequence of catalytic testing at 700 °C and allow conversion rates well above the InDEC-0.56-mm and InHo-0.05-mm anode half-cells even at the lowest temperature of 600 °C (Fig. 4). According to these results, the presence of defects or cracking in the electrolyte layer leads to oxidation reactions not only at the frontal surface and inside the anode chamber, but also in the supposedly inert YSZ electrolyte chamber. The presence of two reacting chambers instead of only one thus results in conversion rates much higher than the expected 50% limit. The next thin film electrolyte half-cell, i.e., the InDEC-0.56-mm anode catalyst, was shown to be crack-free under optical microscopy. However, examination of the anode performance at 700 °C after each sequence of tests at 600 °C and 800 °C rather suggest some cracking of the electrolyte during the 800 °C catalytic testing. Indeed, the methane and oxygen conversion rates at R_{in} = 2.0 were respectively 10 and 20 percentage points higher than recorded earlier in the first sequence of tests at 700 °C. Crack growth at 800 °C could thus explain the progressive raise in the conversion rates observed in Fig. 6 in the sequence from R_{in} = 2.0 to 1.0.

Although we suspect hot spots and thermal stresses to be at the origin of the electrolyte cracking, mechanical stresses from the re-oxidation and reduction processes performed between each sequence of testing cannot be totally ignored. Indeed, such redox cycles lead to large bulk volume changes and thermo-mechanical variations in the Ni-YSZ anode that result in destructive changes to the thin electrolyte film or degradation of the electrochemical performance [39–41].

The above results thus stress the importance of designing a more appropriate entry layout that could at least lower the extent of the thermal gradients and the risk of electrolyte cracking.

3.3. Selectivity

As shown above, an increase in the operating temperature and the CH_4:O_2 flow rate ratio favours the partial oxidation products. However, the presence of total combustion products is confirmed in all conditions. An analysis of the selectivity change as a function of anode thickness, CH_4:O_2 ratio and temperature may shed some light on the reaction processes involved in the single-chamber reactor.

Fig. 8 first presents the general trends observed in S_{H_2} and S_{CO} as a function of R_{in}, using the InHo-0.05-mm anode at 600 °C and 800 °C as an example. At the lowest temperature, the selectivity of both species increases with an increase in R_{in}. According to the anode layers, it is characterized either by a nearly plateau region above R_{in} = 1.2 or, as shown in Fig. 8, by a maximum at R_{in} = 1.6. By rising the operating temperature, a continuous increase in selectivity occurs instead, and the maximum or plateau region disappears. Both types of behaviour were observed before by Schmidt and his colleagues on Ni and Rh catalysts deposited on α-Al_2O_3 [29–31]. Their experiments performed under autothermal conditions resulted in maximum- or plateau-like regions in the case of foam monolith supports or continuous increases in selectivity under fluidized bed conditions. Not only the temperature but also the type of support and quite probably the amount of catalyst it contains may thus affect the selectivity response to H_2 and CO with an increase in the CH_4:O_2 ratios.

Thermodynamic calculations of the methane partial oxidation system suggest that an increase in temperature favours high selectivity to H_2 and CO [42], at least at the highest CH_4:O_2 ratios. 90% and over is thus expected in S_{H_2} and S_{CO} at temperatures above 700 °C. Published data confirm this behaviour, although maximum values may not be reached in the case of kinetically controlled processes [21,23,43,44]. Superior catalysts in the formation of syngas products give rise to a H_2/CO ratio close to the stoichiometric value of 2.0 in the case where complete conversion of oxygen occurs. In the presence of unconverted O_2, however, the final selectivity to H_2 and CO largely depends either on their consecutive oxidation to H_2O and CO_2 [45] or on a combination of catalytic partial oxidation and H_2 oxidation via surface chemistry [46]. Both reaction paths result in significant lowering of the H_2/CO ratios.

Our data in Fig. 8 already suggest that single-chamber reactors may lead to significant departure with regard to the beneficial effects of higher operating temperatures. Indeed, at a CH_4:O_2 ratio of 2.0 and a temperature of 600 °C, for example, selectivity to H_2 and CO is comparable at about 55%. However, at 800 °C, while S_{CO} increases to near 80%, S_{H_2} in fact decreases to 48%. Identical trends occur at every R_{in} value in the case of the InHo-0.05-mm anode. The response to an increase in temperature varies, however, according to the anode layers, especially at the highest R_{in} ratios. This is shown in Fig. 9, where their behaviour is compared at R_{in} = 2.0 and 1.0. At CH_4:O_2 = 2.0, an increase in anode thickness does not affect the enhanced selectivity to CO already observed with the InHo-0.05-mm anode. For hydrogen, however, the continuous decrease in S_{H_2} measured at the InHo-0.05-mm anode between 600 °C and 800 °C

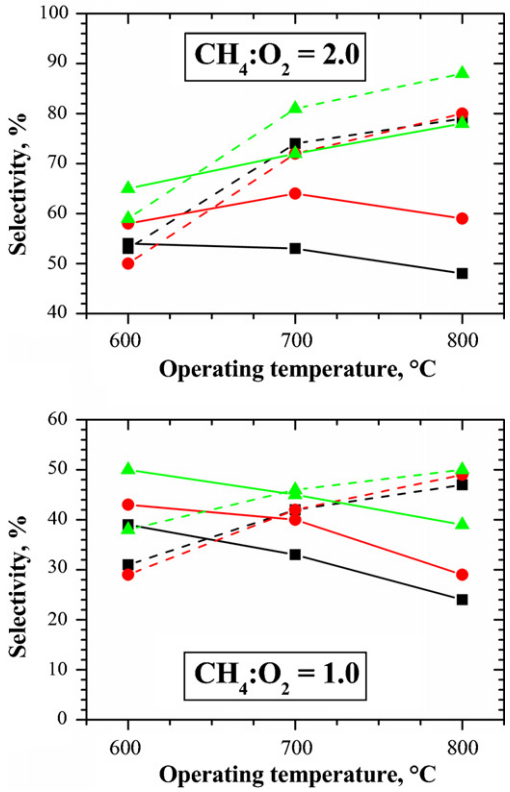

Fig. 9. Selectivity to H_2 and CO for the three anode layer catalysts at CH_4:O_2 = 2.0 and 1.0 as a function of the operating temperature. Solid lines: S_{H_2}; dashed lines: S_{CO}. Black squares: InHo-0.05-mm anode; red circles: InDEC-0.56-mm anode; green triangles: FJ-1.52-mm anode. (For interpretation of the references to color in this figure legend, the reader is referred to the web version of the article.)

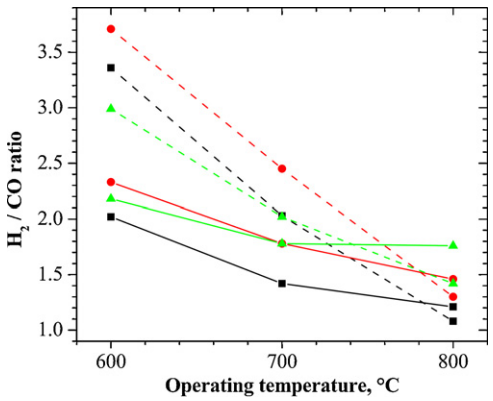

Fig. 10. Variation in the H_2/CO ratio at CH_4:O_2 = 2.0 and 0.8 as a function of the operating temperature. Solid lines: R_{in} = 2.0; dashed lines: R_{in} = 0.8. Black squares: InHo-0.05-mm anode; red circles: InDEC-0.56-mm anode; green triangles: FJ-1.52-mm anode. (For interpretation of the references to color in this figure legend, the reader is referred to the web version of the article.)

is not always matched by the two other catalysts. In the case of the InDEC-0.56-mm anode, S_{H_2} first rises from 600 °C to 700 °C, but this improvement stopped at a higher temperature. Another increase in anode thickness is beneficial, however, and the FJ-1.52-mm anode finally results in the expected response in S_{H_2}, which goes from 65% at 600 °C to 78% at 800 °C. This rise, however, is not as sharp as for selectivity to CO that reaches 88% at 800 °C. With an increase in the O_2 content (Fig. 9, CH_4:O_2 = 1.0), the rise in S_{CO} between 600 °C and 800 °C is levelling out but still present, even in reducing further R_{in} at 0.8. For hydrogen, however, the improvement observed previously on the FJ-1.52-mm anode at R_{in} = 2.0 is rapidly lost and S_{H_2} shows a continuous decrease at the three catalyst layers below R_{in} = 1.6.

The variations in selectivity to hydrogen and carbon monoxide seen above may thus give rise to H_2/CO ratios quite remote from the true stoichiometric value of 2.0 expected from the simple partial oxidation reaction. This is shown in Fig. 10 for the two limiting cases of R_{in} = 2.0 and 0.8. At 0.8, for example, the ratio monotonically decreases from high values above 3.0 at 600 °C to low values below 1.5 at 800 °C. Nevertheless, these data were obtained under QMS conditions that account for the total flow of the gas species at the reactor exit and which only give rise to average values of conversion and selectivity. The partial oxidation of methane, however, is known to occur within at least two mechanistically different zones. Horn et al. [47], for example, confirmed the presence of an oxidation zone at the catalyst entrance followed by a longer reforming zone further downstream. In the oxidation zone, the occurrence of strong exothermic reactions was leading to the production of significant amounts of H_2, CO and H_2O, as well as to the complete conversion of oxygen. At a methane-to-oxygen ratio of 2.0, their high-resolution spatial chemical analyses were giving rise to H_2/CO ratios close to 1.0, in agreement with the preferential oxidation of hydrogen in the presence of residual oxygen [45,46]. These low ratios at the end of the oxidation zone were clearly contrasting with the nearly stoichiometric value of 2.0 they measured at the reactor exit. The rise was shown to come from the flow of both the unconverted CH_4 and the reaction products into the reforming zone where the catalytic processes are now governed by the steam reforming reaction and the water gas shift chemistry [48]. Using a similar combustion and reforming mechanism throughout the reactor length, our data should thus be able to reflect the rises in H_2/CO expected in the reforming zone. Fig. 10 allows a comparison with the observations made by Horn at least considering the results obtained at R_{in} = 2.0 and at the highest temperature of 800 °C where the steam reforming reaction is kinetically favoured. In our case, the thin InHo-0.05-mm anode seems poorly capable of reforming the remaining methane gas species. Indeed, it leads to an H_2/CO ratio of only 1.2, a value that would be more typical of the intense catalytic activity that occurs in the oxidation zone. An increase in the anode thicknesses, however, results in a much better conversion and a rise in H_2/CO. More precisely, the InDEC-0.56-mm and FJ-1.52-mm anodes are reaching values of nearly 1.5 and 1.8, respectively. Under the above conditions, the extent of the steam reforming process along the SC-SOFC anodes proved to be strongly dependent on the thickness of the anode layers, in agreement with the findings made earlier in more conventional dual-chamber SOFC [49]. Moreover, and as shown in Fig. 10 for R_{in} = 0.8, such dependency remains with a decrease in the methane-to-oxygen ratio. As far as the H_2/CO ratios are concerned, however, they are reduced even further, especially below R_{in} = 1.6. This is probably due to an easier reoxidation of the formed hydrogen in the presence of larger amounts of oxygen.

As briefly mentioned earlier and also shown in Fig. 10, a decrease in furnace temperature leads to a general increase in the H_2/CO ratio despite a slowdown of the hydrogen production from the steam reforming reaction. The rise becomes further apparent with a reduction in R_{in} and a drop in temperature below 700 °C. At 600 °C and R_{in} = 0.8, the H_2/CO ratio may even exceed the maximum value of 3.0 expected from the steam reforming reaction alone. This is especially the case for the less efficient InHo-0.05-mm and InDEC-0.56-mm anodes, where the H_2/CO ratios amount to about 3.4 and 3.7, respectively. Presumably, here the increasing production of water from the preferential oxidation of hydrogen in the oxidation zone allows the water gas shift reaction to become the dominant chemical route in the downstream reforming zone. Unlike the previous observations made for the steam reforming reaction at 800 °C,

however, there is no more evidence of gas transport limitation in the Ni-YSZ anode layers. In the low temperature water gas shift regime, the catalytic reaction and the resulting increase in H_2/CO ratio may instead be dependent on catalyst loading and the particle size of the individual contact and functional layers. In this area, however, further work would be required on anode layers, the composition and microstructure of which should be better controlled.

4. Conclusions

In SC-SOFC, the direct internal conversion of the hydrocarbon fuel at the anode component ensures the formation of the electrochemically active H_2 and CO gas species. However, the catalytic performance of the anode depends on multiple structural and operational factors. On commonly used Ni-YSZ cermet, the present study shed some light on the role of anode thickness, the CH_4:O_2 flow rate ratio and the operating temperature.

The general trend toward a reduction in the operating temperature of the solid oxide fuel cells must be carefully examined in the case of the SC-SOFC. Indeed, both the catalytic activity and the production of syngas are reduced significantly at lower temperatures. In certain cases, the yields in the partial and complete oxidation products are found to be just about the same, leading to significant dilution of the H_2 and CO gas species even at high CH_4:O_2 ratios. In such a case, it could be of interest to evaluate the occurrence of any further reduction in the SC-SOFC performance, beyond the one already expected from the simple lowering of the operating temperature.

At elevated temperatures, other precautions must also be taken, however. The possible cracking of the thin electrolyte film in anode-supported cells when hot spots are present at the fuel cell entrance must be carefully considered. In SC-SOFC, special attention must thus be given to the temperature gradients at the reactor entrance as well as to the heat transfer processes throughout the reactor. In reducing the thermal stresses in the membrane electrolyte assembly, a longer fuel cell life is expected. Anode thickness must also be carefully examined since the use of thin layers leads to a significant reduction in hydrogen species at the reactor exit and to a lowering in the H_2/CO ratios. As hydrogen is generally considered the most active electrochemical species, this may lead to reduced electrical performance of the complete fuel cells.

The present results finally show that any further optimization of the SC-SOFC goes through even more catalytic studies of its electrode materials under real structure and morphology as well as final reactor configuration.

Acknowledgements

The authors gratefully acknowledge Forschungszentrum Jülich for its supply of half-cells.

References

[1] T. Hibino, H. Tsunekawa, S. Tanimoto, M. Sano, J. Electrochem. Soc. 147 (2000) 1338–1343.
[2] I.C. Stefan, C.P. Jacobson, S.J. Visco, L.C. De Jonghe, Electrochem. Solid State Lett. 7 (2004) A198–A200.
[3] T.W. Napporn, X. Jacques-Bédard, F. Morin, M. Meunier, J. Electrochem. Soc. 151 (2004) A2088–A2094.
[4] B.E. Buergler, M.E. Siegrist, L.J. Gauckler, Solid State Ionics 176 (2005) 1717–1722.
[5] T. Suzuki, P. Jasinski, V. Petrovsky, H.U. Anderson, F. Dogan, J. Electrochem. Soc. 152 (2005) A527–A531.
[6] M. Yano, A. Tomita, M. Sano, T. Hibino, Solid State Ionics 177 (2007) 3351–3359.
[7] T. Hibino, S. Wang, S. Kakimoto, M. Sano, Electrochem. Solid State Lett. 2 (1999) 317–319.
[8] Z. Shao, S.M. Haile, J. Ahn, P.D. Ronney, Z. Zhan, S.A. Barnett, Nature 435 (2005) 795–798.
[9] Y. Hao, Z. Shao, J. Mederos, W. Lai, D.G. Goodwin, S.M. Haile, Solid State Ionics 177 (2006) 2013–2021.
[10] M. Hori, K. Nagasaka, M. Miyayama, G. Trunfio, E. Traversa, Key Eng. Mater. 301 (2006) 155–158.
[11] Z. Shao, C. Kwak, S.M. Haile, Solid State Ionics 175 (2004) 39–46.
[12] I. Riess, J. Power Sources 175 (2008) 325–337.
[13] B. Morel, R. Roberge, S. Savoie, T.W. Napporn, M. Meunier, Appl. Catal. A 323 (2007) 181–187.
[14] Y. Hao, D.G. Goodwin, J. Electrochem. Soc. 154 (2007) B207–B212.
[15] Y. Hao, D.G. Goodwin, J. Electrochem. Soc. 155 (2008) B666–B674.
[16] M. Kuhn, T.W. Napporn, Energies 3 (2010) 57–134.
[17] B. Morel, R. Roberge, S. Savoie, T.W. Napporn, M. Meunier, Electrochem. Solid State Lett. 10 (2007) B31–B33.
[18] B. Morel, R. Roberge, S. Savoie, T.W. Napporn, M. Meunier, J. Power Sources 186 (2009) 89–95.
[19] B. Morel, S. Savoie, R. Roberge, T.W. Napporn, M. Meunier, in: U. Bossel (Ed.), 7th European SOFC Forum Conference CD, Lucerne, Switzerland, July 2006, p. P1105.
[20] Y.H. Hu, E. Ruckenstein, in: B.C. Gates, H. Knoezinger (Eds.), Advances in Catalysis, Academic Press, New York, 2004, pp. 297–345.
[21] A.P.E. York, T. Xiao, M.L.H. Green, Top. Catal. 22 (2003) 345–358.
[22] D. Dissanayake, M.P. Rosynek, K.C.C. Kharas, J.H. Lunsford, J. Catal. 132 (1991) 117–127.
[23] W.J.M. Vermeiren, E. Blomsma, P.A. Jacobs, Catal. Today 13 (1992) 427–436.
[24] V.R. Choudhary, A.M. Rajput, B. Prabhakar, Catal. Lett. 15 (1992) 363–370.
[25] F. van Looij, J.W. Geus, J. Catal. 168 (1997) 154–163.
[26] Y.H. Hu, E. Ruckenstein, J. Phys. Chem. A 102 (1998) 10568–10571.
[27] Z.-W. Liu, K.-W. Jun, H.-S. Roh, S.-C. Baek, S.-E. Park, J. Mol. Catal. A: Chem. 189 (2002) 283–293.
[28] C. Zhang, L. Sun, R. Ran, Z. Shao, Electrochem. Commun. 11 (2009) 1563–1566.
[29] D.A. Hickman, E.A. Haupfear, L.D. Schmidt, Catal. Lett. 17 (1993) 223–237.
[30] S.S. Bharadwaj, L.D. Schmidt, J. Catal. 146 (1994) 11–21.
[31] P.M. Torniainen, X. Chu, L.D. Schmidt, J. Catal. 146 (1994) 1–10.
[32] G. Landi, P.S. Barbato, S. Cimino, L. Lisi, G. Russo, Catal. Today 155 (2010) 27–34.
[33] X. Jacques-Bédard, T.W. Napporn, R. Roberge, M. Meunier, J. Power Sources 153 (2006) 108–113.
[34] G. Veser, J. Frauhammer, Chem. Eng. Sci. 55 (2000) 2271–2286.
[35] M. Maestri, A. Beretta, G. Groppi, E. Tronconi, P. Forzatti, Catal. Today 105 (2005) 709–717.
[36] B. Kimmerle, J.-D. Grunwaldt, A. Baiker, P. Glatzel, P. Boye, S. Stephan, C.G. Schroer, J. Phys. Chem. C 113 (2009) 3037–3040.
[37] A. Beretta, G. Groppi, M. Lualdi, I. Tavazzi, P. Forzatti, Ind. Eng. Chem. Res. 48 (2009) 3825–3836.
[38] O.P. Klenov, S.A. Pokrovskaya, N.A. Chumakova, S.N. Pavlova, V.A. Sadykov, A.S. Noskov, Catal. Today 144 (2009) 258–264.
[39] D. Waldbillig, A. Wood, D.G. Ivey, Solid State Ionics 176 (2005) 847–859.
[40] Y. Zhang, B. Liu, B. Tu, Y. Dong, M. Cheng, Solid State Ionics 176 (2005) 2193–2199.
[41] J. Laurencin, G. Delette, B. Morel, F. Lefebvre-Joud, M. Dupeux, J. Power Sources 192 (2009) 344–352.
[42] B.C. Enger, R. Lødeng, A. Holmen, Appl. Catal. A 346 (2008) 1–27.
[43] A. Beretta, T. Bruno, G. Groppi, I. Tavazzi, P. Forzatti, Appl. Catal. B 70 (2007) 515–524.
[44] Y. Wang, W. Wang, X. Hong, Y. Li, Z. Zhang, Int. J. Hydrogen Energy 34 (2009) 2252–2259.
[45] A. Donazzi, A. Beretta, G. Groppi, P. Forzatti, J. Catal. 255 (2008) 241–258.
[46] A.B. Mhadeshwar, D.G. Vlachos, J. Phys. Chem. B 109 (2005) 16819–16835.
[47] R. Horn, K.A. Williams, N.J. Degenstein, A. Bitsch-Larsen, D. Dalle Nogare, S.A. Tupy, L.D. Schmidt, J. Catal. 249 (2007) 380–393.
[48] B.C. Michael, A. Donazzi, L.D. Schmidt, J. Catal. 265 (2009) 117–129.
[49] J. Laurencin, F. Lefebvre-Joud, G. Delette, J. Power Sources 177 (2008) 355–368.